ACS Energy LETTERS

http://pubs.acs.org/journal/aelccp

LETTER

High-Performance Ultrathin $BiVO_4$ Photoanode on Textured Polydimethylsiloxane Substrates for Solar Water Splitting

Jiheng Zhao,[†] Yu Guo,[‡] Lili Cai,[†] Hong Li,[†] Ken Xingze Wang,[‡] In Sun Cho,[§] Chi Hwan Lee,[∥] Shanhui Fan,[‡] and Xiaolin Zheng*[,†]

[†]Department of Mechanical Engineering and [‡]Department of Electrical Engineering, Stanford University, Stanford, California 94305, United States

[§]Department of Materials Science & Engineering and Energy Systems Research, Ajou University, Suwon 443-749, South Korea

[∥]School of Mechanical Engineering, Weldon School of Biomedical Engineering, Purdue University, West Lafayette, Indiana 47907, United States

Supporting Information

ABSTRACT: Photoelectrochemical (PEC) water splitting devices rely on light-absorbers to absorb sunlight, and the photogenerated electrons and holes further react with water to generate hydrogen and oxygen. Fabricating light-absorbers on textured substrates offers alternative routes for optimizing their PEC performance. Textured substrates would greatly enhance both light absorption and surface reactions of photoanodes and thus reduce the total amount of light-absorbers needed. Herein, we report the fabrication of ultrathin $BiVO_4$ photoanode film on textured polydimethylsiloxane (PDMS) substrates by using a modified water-assisted transfer printing method. Significantly, a pristine $BiVO_4$ photoanode of only 80 nm thick shows a photocurrent density of 1.37 mA/cm^2 at 1.23 V_{RHE} on patterned PDMS substrates, which is further increased to ~2.0 mA/cm^2 at 1.23 V_{RHE} when FeOOH oxygen evolution catalyst is added. We believe that our transfer printing method can be broadly applied to integrate photoelectrodes and other thin-film optoelectronic devices (e.g., solar cells and electronics) onto diverse textured substrates to enhance their performance.

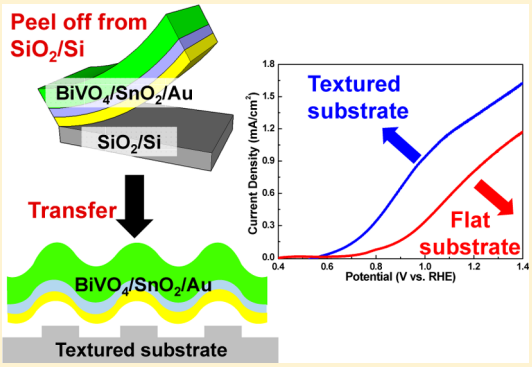

Photoelectrochemical (PEC) water splitting devices depend on light-absorbers to absorb sunlight, and the photogenerated electrons and holes further react with water to generate hydrogen and oxygen. Efficient PEC devices demand simultaneous high light absorption, charge separation, and charge-transfer efficiencies. Currently, most light-absorbers are fabricated on flat conductive substrates (e.g., fluorine-doped SnO_2 coated glass, FTO); hence, most efforts on improving photoelectrodes have been focused on optimizing the light-absorbers themselves, such as engineering their nanostructures to maximize light absorption while reducing minority carrier diffusion distance,[1] modifying their chemical compositions by doping to change their charge transport[2,3] and charge-transfer properties,[4−6] and adding plasmonic metal nanoparticles to enhance light absorption.[7,8]

Instead, fabricating light-absorbers on surface-textured substrates offers alternative routes for optimizing photoelectrodes for enhanced PEC performance.[9] Light-absorbers have been coated onto transparent-conductive oxide nanowire arrays that aim to improve the charge transport efficiency while maintaining efficient light absorption and large surface area.[10,11] Recently, light-absorbers were directly deposited on optically designed textured substrates for efficient light trapping while reducing the charge transport distance.[12−15] For example, a 26 nm thick Co-decorated Ti-doped α-Fe_2O_3 film was deposited by pulse laser deposition on a V-shaped gold−silver coated glass, and it achieves about 0.4 mA/cm^2 at 1.23 V_{RHE} due to both resonant light trapping and light retrapping effects.[12]

All these previous integrations of light-absorbers with surface-textured substrates were realized by directly depositing light-absorbers onto textured substrates.[12,13] Nevertheless, surface-textured substrates can be expensive to synthesize or fabricate. Also, the deposition conditions of light-absorbers further limit the material choice of the textured substrates. In addition, it could be difficult to achieve conformal coating of

Received: March 25, 2016
Revised: April 20, 2016
Accepted: April 22, 2016

DOI: 10.1021/acsenergylett.6b00032
ACS Energy Lett. 2016, 1, 68−75

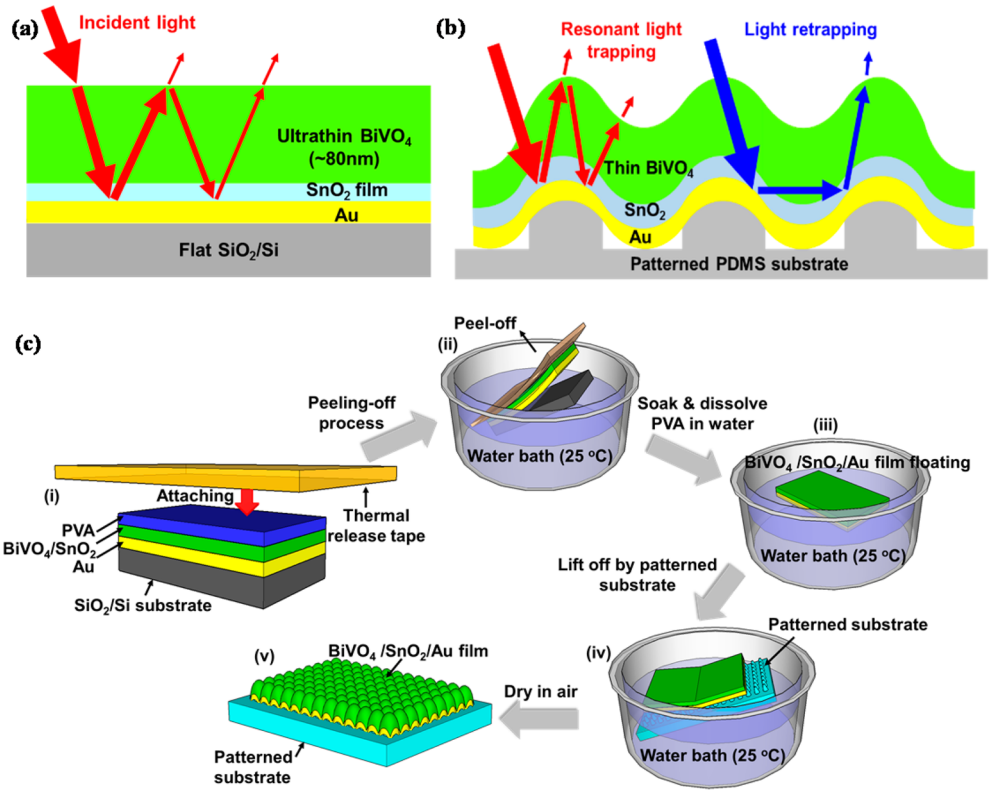

Figure 1. Schematic illustration of the design rationales and the transfer process for integrating $BiVO_4$ onto patterned PDMS substrates. (a) Enable resonant light trapping by adding Au underneath $BiVO_4$. (b) Patterned PDMS substrates enable both resonant light trapping and light retrapping and increase the surface roughness factor. (c) Schematic of the modified water-assisted transfer printing process: (i) spin coating PVA protection layer and attaching TRT on top of $BiVO_4$; (ii) the $BiVO_4/SnO_2/Au$ film is peeled off from SiO_2/Si wafer in a water bath; (iii) dissolving PVA layer in water to separate the photoanode from TRT; (iv) the floating $BiVO_4/SnO_2/Au$ film is fished out by a patterned PDMS substrate; and (v) the $BiVO_4/SnO_2/Au$ film is textured on the patterned PDMS because of the capillary force induced by water drying.

light-absorbers onto textured substrates. Those challenges can be alleviated by developing alternative methods for integrating light-absorbers with textured substrates. Herein, we report the use of a modified water-assisted transfer printing method[16−18] (WTP) to integrate light-absorbers with surface-textured substrates. We demonstrated this new approach by using a bismuth vanadate ($BiVO_4$) photoanode as a model system because $BiVO_4$ (bandgap, ~2.4 eV), when deposited on flat FTO substrates, has exhibited great PEC performance with high photocurrent densities and low onset potentials.[1,3,19,20] We used patterned PDMS substrates to represent a challenging surface-textured substrate for PEC because existing methods cannot directly deposit light-absorbers onto PDMS substrates. In addition, PDMS substrates are transparent, flexible, and easy to fabricate with diverse surface patterns. Those capabilities of PDMS substrates will facilitate the optimization and integration of photoelectrodes to form tandem cell systems. Significantly, our transferred $BiVO_4$ film (~80 nm) on patterned PDMS substrates achieves a photocurrent density of ~2.0 mA/cm^2 at 1.23 V_{RHE}, which is comparable or even better than those of typical $BiVO_4$ films (200 nm or thicker) deposited on FTO substrates in the literature.[3,7,21,22]

Figure 1 illustrates the design rationales and the transfer process for integrating $BiVO_4$ onto patterned PDMS substrates. Integration of $BiVO_4$ onto patterned PDMS substrates not only increases the surface roughness factor but also enables the implementation of a dual light-trapping strategy.[12] The first light-trapping strategy is based on resonant light trapping,[12] for which a gold (Au) film is added beneath $BiVO_4/SnO_2$ (hole blocking layer) as a current collector and back reflector (Figure 1a). As such, an optical cavity is formed within the ultrathin $BiVO_4/SnO_2$ film that enhances the light absorption by increasing the light intensity and photon lifetime in the film. The increase of photon lifetime is due to the reduced leakage rate of photons into the Si substrate underneath the gold layer. The second light-trapping strategy is based on light retrapping among the surface-textured $BiVO_4/SnO_2$ film, for which some of the escaped back-reflected photons from the ultrathin film are redirected into the film and absorbed (Figure 1b).

Figure 1c illustrates the process of transferring the ultrathin $BiVO_4/SnO_2$ film from Si wafers onto patterned PDMS substrates. First, a 300 nm thick Au film was deposited onto a SiO_2/Si wafer by electron beam evaporation, and thin films of SnO_2 and $BiVO_4$ (~80 nm; see Figure S1 for thickness optimization) were then spin coated on top of the Au film (Figure 1a). The Au film serves as the back electron collector and light reflector, and Au was chosen for its high electrical conductivity, good chemical compatibility, and thermal stability during the fabrication conditions of $BiVO_4$. The thin SnO_2 layer (~10 nm) serves as a selective electron transport layer because of the large valence band offset between SnO_2 and $BiVO_4$, which blocks the hole injection into the Au film and hence reduces the interfacial charge recombination.[20,23,24] Next, a thin layer of water-soluble poly(vinyl alcohol) (PVA) was spin coated on top of $BiVO_4$. On top of PVA, a thermal release tape (TRT, NittoDenko) was further attached serving as a temporary transfer holder (Figure 1c (i)). Then the entire structure (TRT/PVA/$BiVO_4/SnO_2$/Au) was peeled off from

DOI: 10.1021/acsenergylett.6b00032
ACS Energy Lett. 2016, 1, 68−75

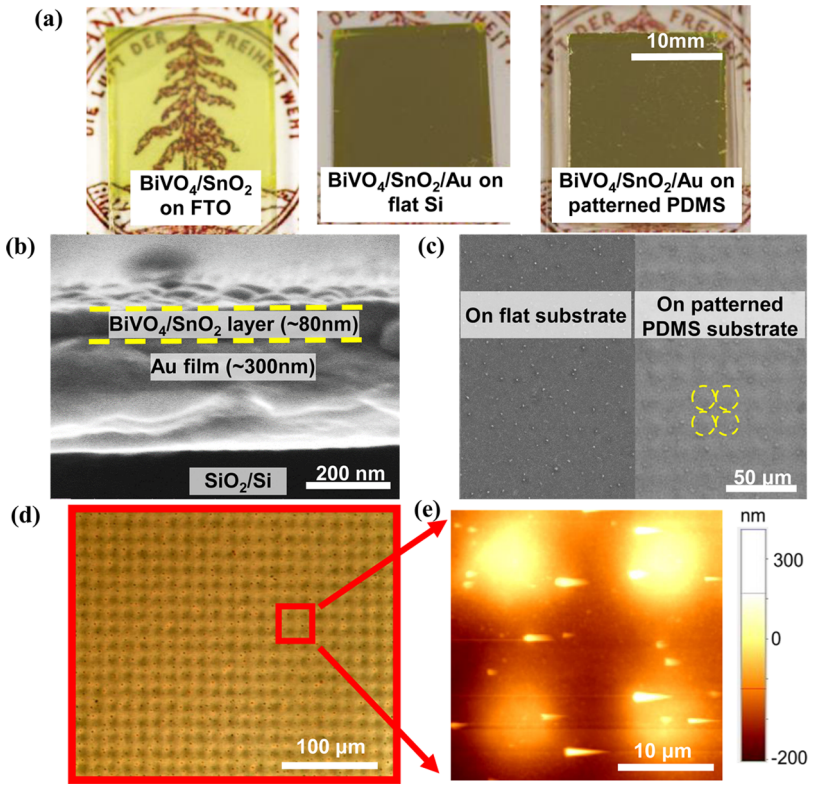

Figure 2. Morphology characterization of various $BiVO_4$ photoanodes. (a) Photographs of $BiVO_4/SnO_2$/FTO (left), $BiVO_4/SnO_2$/Au on flat Si wafer (middle), and $BiVO_4/SnO_2$/Au on patterned PDMS (right). (b) Cross-sectional SEM image of $BiVO_4/SnO_2$/Au film on the Si wafer before transfer. (c) Top-view SEM images of $BiVO_4/SnO_2$/Au film before and after the transfer to a 9 μm rod PDMS substrate. (d) Optical microscope image of $BiVO_4/SnO_2$/Au film on a 9 μm rod PDMS substrate. (e) AFM image of the transferred $BiVO_4/SnO_2$/Au film on a 9 μm rod PDMS substrate.

the SiO_2/Si wafer in water at room temperature (Figure 1c (ii)). Here, the Au film, similar to the Ni film in the original WTP method,[9,16−18] can be easily peeled off from the SiO_2/Si wafer. In addition, we replaced the poly(methyl methacrylate) in the original WTP method with water-soluble PVA as a protection layer to avoid contamination and damage to the ultrathin $BiVO_4$ film during the transfer process. Then, the peeled off TRT/PVA/$BiVO_4/SnO_2$/Au film was soaked in the water bath for a few hours to fully dissolve the water-soluble PVA layer (Figure 1c (iii)), and the TRT is consequently lifted off as well. The remaining $BiVO_4/SnO_2$/Au film naturally floats on the water surface and can be fished out by patterned PDMS substrates (Figure 1c (iv)). Finally, the entire substrate was dried in air, and the capillary force induced by water evaporation pulls down the $BiVO_4/SnO_2$/Au film to follow the topography of the patterned PDMS substrates (Figure 1c (v)).[25]

Figure 2a shows three types of control samples of $BiVO_4$ films that we used to study the effect of surface-textured substrates on the PEC performance. The first type is a flat yellowish $BiVO_4/SnO_2$ thin film on FTO, which is the most common configuration for PEC study. The second and third types are the $BiVO_4/SnO_2$/Au thin film on a flat Si substrate and on a patterned PDMS substrate, corresponding to before and after the transfer process, respectively. The detailed morphology of the $BiVO_4/SnO_2$/Au film before and after the transfer were examined by using scanning electron microscopy (SEM) (Figure 2b,c), optical microscopy (Figure 2d), and atomic force microscopy (AFM) (Figure 2e). The $BiVO_4/SnO_2$ film is about 80 nm thick (Figure 2b) and rather flat and uniform on the Au-coated SiO_2/Si wafer before transfer (Figure 2c, left). The $BiVO_4$ film is composed of densely packed monoclinic phase $BiVO_4$ nanoparticles around 100 nm in diameter (Figures S2 and S3). After being transferred to PDMS, the $BiVO_4/SnO_2$ film exhibits patterns of brightness contrast that follow the underlying PDMS pattern (right SEM image in Figure 2c,d). The AFM topography measurement confirms that the transferred $BiVO_4/SnO_2$/Au film follows the topography of the PDMS pattern (9 μm rod pillar substrate, Figure 2d) and its peak and valley height difference is about 500 nm (Figure 2e). All of these results confirm that the modified WTP method has successfully transferred and further textured the $BiVO_4/SnO_2$/Au film on patterned PDMS substrates.

Figure 3 compares the PEC performance of the three types of $BiVO_4$ photoanodes shown in Figure 2a. First, the typical $BiVO_4/SnO_2$/FTO configuration used for PEC photoanode (Figure 2a, left) has the lowest photocurrent density (0.34 mA/cm^2 at 1.23 V_{RHE}) (Figure 3a). Second, by adding the Au film underneath $BiVO_4/SnO_2$ for resonant light trapping (Figure 2a, middle), the photocurrent density is increased to 0.87 mA/cm^2 at 1.23 V_{RHE}, about 2.6 times of the control sample on FTO without Au (Figure 3a). It should be noted that we deposited Au on flat Si wafers instead of FTO because the flat Si surface is needed for the following WTP process. Because the Au film is very reflective and inert, the underlying Si wafer with a 300 nm thick SiO_2 top layer has no contribution to the PEC performance. Third, after being transferred to the patterned light retrapping PDMS substrate, the photocurrent density of the $BiVO_4/SnO_2$/Au/patterned PDMS (9 μm rod, Figure 2c, right) reaches 1.37 mA/cm^2 at 1.23 V_{RHE} (Figure 3a), which is

DOI: 10.1021/acsenergylett.6b00032
ACS Energy Lett. 2016, 1, 68−75

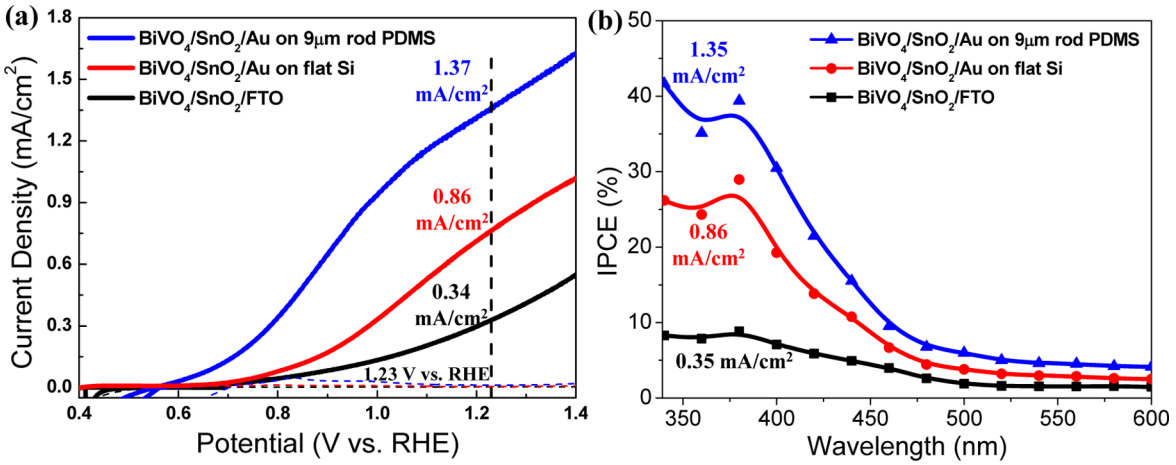

Figure 3. Comparison of photoelectrochemical performance of $BiVO_4$ photoanode on different substrates. (a) Current density−voltage (J−V) curves (solid lines, under simulated AM 1.5G illumination; dotted lines, dark conditions) and (b) incident photon-to-current efficiency (IPCE) measured at 1.23 V_{RHE} for the control $BiVO_4/SnO_2$/FTO sample, the flat $BiVO_4/SnO_2$/Au film on Si wafers, and the textured $BiVO_4/SnO_2$/Au film on a 9 μm rod-patterned PDMS substrate. The current densities listed are integrated from IPCE over standard AM 1.5G spectrum, and they match well the measured photocurrent densities.

around three times and 60% higher than those of the first and second control samples, respectively. The photocurrent density of $BiVO_4/SnO_2$/Au/patterned PDMS is quite high considering the facts that the $BiVO_4$ film here is of low quality, made by the sol−gel method without any doping or surface modification, and is only about 80 nm thick, which is much smaller than the light absorption depth for $BiVO_4$ (~200−500 nm).[22,26] We have also transferred $BiVO_4/SnO_2$/Au film to a FTO substrate. The PEC performance of $BiVO_4/SnO_2$/Au/FTO photoanode is very similar to that of $BiVO_4/SnO_2$/Au/Si (Figure S4), which shows the effectiveness of surface texturing in improving the PEC performance. Finally, the integrated photocurrent densities from the incident photon-to-current conversion efficiency (IPCE) measurement (at 1.23 V_{RHE}) over standard AM 1.5G spectrum are 0.35, 0.86, and 1.35 mA/cm^2 (Figure 3b), respectively, which match very well with the measured photocurrent densities (Figure 3a), confirming the accuracy of our PEC characterization. The IPCE is increased with application of each light-trapping scheme over a broad wavelength range, confirming the successful implementation of two light-trapping schemes through our transfer-based approach.

Because the textured PDMS substrates potentially affect both light absorption and surface roughness factor, we first quantify the light absorption enhancement from the dual light-trapping scheme. Figure 4a compares the light absorption of three types of $BiVO_4$ photoanodes (Figure 2a): the control flat sample of $BiVO_4/SnO_2$/FTO, the flat $BiVO_4/SnO_2$/Au film on Si wafers, and the textured $BiVO_4/SnO_2$/Au film on patterned PDMS substrates. First, the light absorption spectra of all three $BiVO_4$ samples exhibit an absorption onset around 520 nm that matches the $BiVO_4$ bandgap of 2.4 eV. Second, the control sample on FTO has the lowest amount of light absorption, as expected, because of its thin thickness around 80 nm. The amount of light absorption is increased by 10−15% by addition of Au and another 5−7% by texturing the film. To further validate our light absorption measurements, we also calculated the light absorption of these three films using the rigorous coupled wave analysis (RCWA)[27] with experimentally measured refractive index for $BiVO_4$ (Figure 4b, inset) and Au by spectroscopic ellipsometry. The calculated light absorption agrees with the experimental results very well in terms of the light absorption onset wavelength and the relative amount of light absorption increase. To see the origin of light absorption increase from the flat substrate to the patterned substrate, we plotted the electric field distribution of both structures at a wavelength of 400 nm in Figure 4c. The electric field distribution of the textured film shows clear diffraction patterns. Because the textured film has a periodicity larger than the wavelength, it operates as a 2D grating that causes the diffraction pattern. In addition, the electric field in the textured $BiVO_4$ film is also higher than that in the flat film, which confirms the light-trapping effects and its associated higher light absorption.

We then quantify the contribution from light absorption increase to the overall PEC performance enhancement for several different PDMS patterns. In Figure 4d, the black circles are the measured PEC photocurrent density increase $\Delta J_{\text{increase,PEC measurement}}$ at 1.23 V_{RHE} before and after the transfer process for four different PDMS patterns, including 6 μm rods, 9 μm rods, 9 μm ribbons, and 15 μm square pillars, and the associated error bars are indications of sample variation. The amount of photocurrent density increase shows a weak dependence on the PDMS patterns; this is because all those patterns are at the micrometer scale. The red triangles in Figure 4d are the calculated maximum possible photocurrent density increase from light absorption enhancement ($\Delta J_{\text{increase,light absorption}}$) by assuming the absorbed photon-to-current efficiency (APCE) being 1 and using the following equation:

$$\Delta J_{\text{increase, light absorption}} = \int_{300\text{ nm}}^{520\text{ nm}} \Delta\eta_{\text{abs}}(\lambda)\, P(\lambda)\, \mathrm{d}\lambda$$

where $\Delta\eta_{\text{abs}}(\lambda)$ is the measured light absorption increase between the flat $BiVO_4/SnO_2$/Au film on Si wafers and the deformed $BiVO_4/SnO_2$/Au film on patterned PDMS substrates at the wavelength of λ (Figure 4a) and $P(\lambda)$ is the incident light intensity at λ under standard 1 sun AM 1.5G. As shown in Figure 4d, $\Delta J_{\text{increase,light absorption}}$ (red triangles) is consistently smaller than $\Delta J_{\text{increase,PEC measurement}}$ (black circles) for all four PDMS patterns. This suggests that light absorption enhancement (Figure 4d) is responsible for around 60%

DOI: 10.1021/acsenergylett.6b00032
ACS Energy Lett. 2016, 1, 68−75

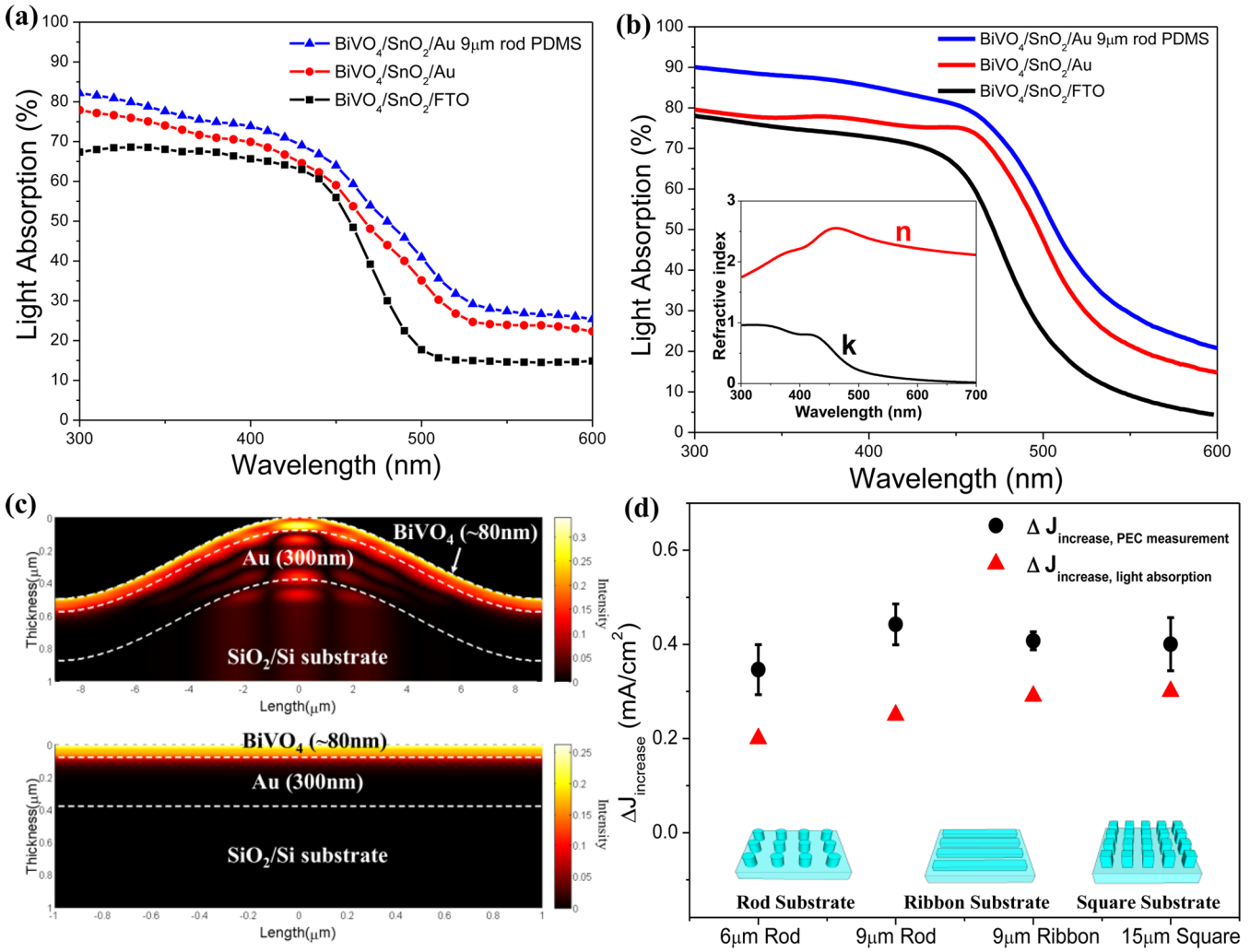

Figure 4. Quantification of the amount of light absorption enhancement by each light-trapping scheme and their impact on photocurrent density. (a) Experimentally measured and (b) numerically calculated light absorption of $BiVO_4$ photoanodes on different substrates (inset: measured refractive index of the $BiVO_4$ film). (c) Normalized electric field distribution of the structures at wavelength 400 nm. Upper panel, $BiVO_4$ on patterned Au substrate; lower panel, $BiVO_4$ on flat Au substrate. (d) The experimentally measured PEC photocurrent density increase ($\Delta J_{\text{increase,PEC measurement}}$, black circles) is larger than that of the estimated maximum possible photocurrent increase from light absorption increase ($\Delta J_{\text{increase,light absorption}}$, red triangles) at 1.23 V_{RHE} before and after the transfer for four different PDMS patterns, including 6 μm rods, 9 μm rods, 9 μm ribbons, and 15 μm square pillars. This suggests that light absorption enhancement is only partially responsible for the PEC performance enhancement on textured PDMS substrates.

$\left(\frac{\Delta J_{\text{increase,light absorption}}}{\Delta J_{\text{increase,PEC measurement}}} \approx \frac{0.24}{0.4} = 60\%\right)$ of the PEC performance enhancement on the textured PDMS substrates.

Next, we examine the PEC performance enhancement from the increased electrochemically active surface area (ECSA) due to the textured substrate. We first estimated the relative reactive surface area ratio before and after transfer by measuring the capacitance ratio ($C_{BiVO_4/\text{flat}}/C_{BiVO_4/\text{patterned}}$) using the cyclic voltammetry (CV) method (Figure S5). Figure 5a plots the capacitive current as a function of the scan rate, and its slope is proportional to capacitance and ECSA (Figure S5).[28,29] The slope for $BiVO_4$ on patterned PDMS is about twice that of $BiVO_4$ on flat Si, suggesting that the ECSA of $BiVO_4$ is doubled after being transferred to patterned PDMS.[28] We also conducted electrochemical impedance spectroscopy (EIS) measurements to evaluate the charge-transfer resistance across various interfaces before and after the transfer. Figure 5b compares the Nyquist plots of the control $BiVO_4/SnO_2/FTO$ sample, the flat $BiVO_4/SnO_2/Au$ film on Si wafers, and the textured $BiVO_4/SnO_2/Au$ film on patterned PDMS substrates. All three samples are modeled with the same equivalent circuit (inset of Figure 5b) based on a midgap charge carrier-trapping mechanism,[22,30] where R1 represents the series resistance and R2 represents the resistance of trapping and detrapping electrons in and out of the mid gap state; Q2 represents the pseudocapacitance of the space charge region; R3 and Q3 represent the charge-transfer resistance and constant phase element between $BiVO_4$ and the electrolyte. First, the addition of Au reduces the series resistance R1 because of the higher electrical conductivity of Au and potential Au doping into SnO_2.[31] Second, the addition of Au also significantly lowers R2 and R3, indicating that the presence of Au improves the quality of $BiVO_4$ by reducing overall charge-transfer resistance within $BiVO_4$ and substrates and improving its interface with electrolyte. Finally, surface texture also reduced R3 as expected because of the increased ECSA. The EIS results indicate that

DOI: 10.1021/acsenergylett.6b00032
ACS Energy Lett. 2016, 1, 68−75

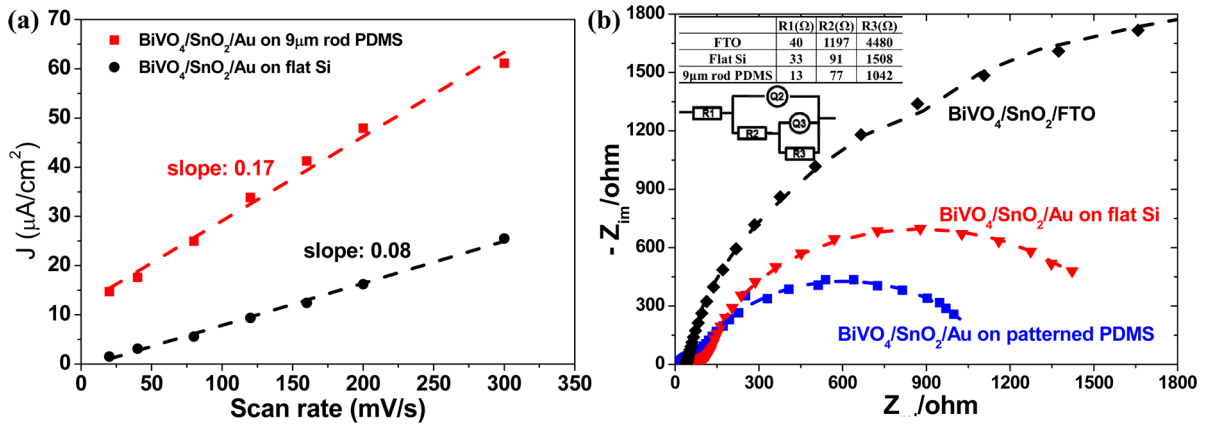

Figure 5. Effects of textured substrates on the charge-transfer efficiency. (a) Capacitive current versus scan rate for ultrathin $BiVO_4$ photoanodes before (on flat Si) and after transfer (on patterned PDMS). (b) Electrochemical impedance spectra of ultrathin $BiVO_4$ photoanodes on different substrates. The dashed lines are the fitted curve based on the proposed equivalent circuit (inset).

the combination of Au and textured substrates reduces the charge-transfer resistance across various interfaces.

In addition, the XRD spectrum after the transfer process shows a new $BiVO_4$ (220) peak (Figure S2), for which {110} facets of $BiVO_4$ have been suggested to have faster hole transfer for the water oxidation reactions.[32] The new exposed (220) plane might be caused by the bending or crack formation when texturing the ultrathin $BiVO_4$ film (Figure S3). The combined CV, EIS, and XRD analyses suggest that adding Au and transferring $BiVO_4$ onto textured substrates increase the charge-transfer efficiency, which is responsible for $\Delta J_{\text{increase,PEC measurement}} > \Delta J_{\text{increase,light absorption}}$ as observed in Figure 4c.

The PEC performance of our ultrathin $BiVO_4$ photoanode on textured PDMS substrates can be further improved by coupling with oxygen evolution catalysts (OECs). Specially, iron oxyhydroxide (FeOOH) as an OEC was directly deposited on top of $BiVO_4$ photoanodes by a simple modified hydrothermal method. Figure 6 shows that after the deposition

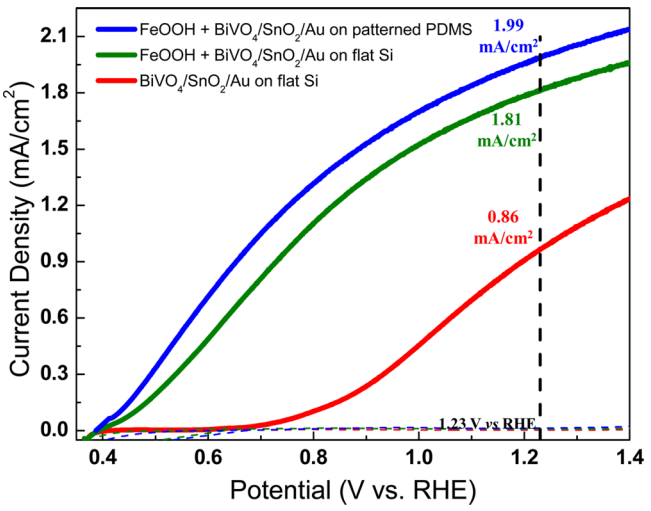

Figure 6. Effects of adding FeOOH as an OEC on the photoelectrochemical performance of $BiVO_4$ photoanode on different substrates. The $J-V$ curves of $BiVO_4/SnO_2/Au$ on flat Si wafer without FeOOH (red) and with FeOOH (green), and $BiVO_4/SnO_2/Au$ on the 9 μm rod pillar PDMS substrate with FeOOH (blue).

of FeOOH, the photocurrent density of our ultrathin flat $BiVO_4/SnO_2/Au$ film reaches 1.81 mA/cm^2 at 1.23 V_{RHE}, which is more than twice that of the sample without FeOOH and six times that of $BiVO_4$ on FTO (Figure 3a). Moreover, after the ultrathin $BiVO_4$ photoanode with FeOOH on the top is transferred to the patterned PDMS substrate (9 μm rod pillar), the photocurrent density reaches 1.99 mA/cm^2 at 1.23 V_{RHE}. If we assume that the charge separation efficiency is nearly 100% in the presence of FeOOH, the photocurrent density increase (1.99 − 1.81 = 0.19 mA/cm^2) after the transfer can be attributed to the light absorption increase. The value of 0.19 mA/cm^2 matches well with the estimated photocurrent density increase based on light absorption only (0.22 mA/cm^2, Figure 4c, red triangle). This again confirms that transferring $BiVO_4$ onto textured PDMS improves both light absorption and charge-transfer efficiency.

Finally, the PEC performance of our ultrathin $BiVO_4$ films was compared to those of pristine $BiVO_4$ photoanodes reported in the literature,[2,3,7,21−23,33−40] as shown in Figure 7. For pristine $BiVO_4$ photoanodes, the optimal thickness is between 200 and 500 nm without light trapping.[22,26] Our control sample of $BiVO_4/SnO_2/FTO$ has low photocurrent density, similar to others. However, the textured ultrathin $BiVO_4/SnO_2/Au$ film on patterned PDMS substrates has a photocurrent density higher than that of all the other pristine $BiVO_4$ photoanodes within the optimal thickness range. Pristine $BiVO_4$ photoanode is known to have poor stability. We also tested the stability of our $BiVO_4/SnO_2/Au$ photoanode on patterned PDMS substrates at 1.23 V_{RHE} under standard AM 1.5G 1 sun illumination condition, which also shows degrading behavior with time (Figure S6).

In conclusion, we demonstrated that fabricating light-absorbers on textured substrates is another effective approach for optimizing their PEC performance. To enable the use of diverse textured substrates, we developed a modified water-assisted transferring printing method by using Au as a separation layer and successfully applied this method to integrate thin $BiVO_4$ film onto patterned PDMS substrates. The combination of Au addition with surface texture enables the application of both resonant light trapping and light retrapping to increase the light absorption. Such combination also reduces the charge-transfer resistance across various interfaces. As a result, the photocurrent density of the 80 nm pristine $BiVO_4$ film is increased by about four times, reaching

DOI: 10.1021/acsenergylett.6b00032
ACS Energy Lett. 2016, 1, 68−75

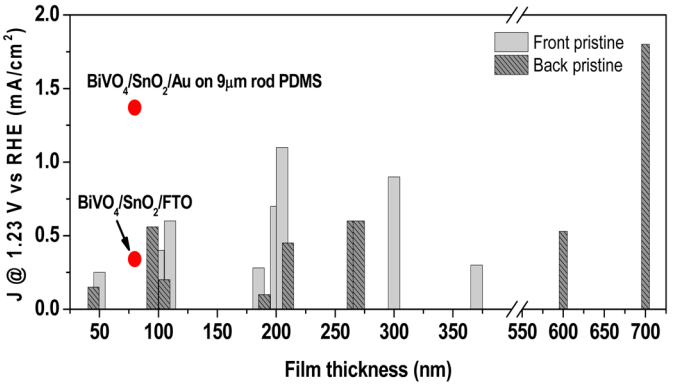

Thickness (nm)	J@1.23V vs RHE pristine $BiVO_4$	Reference
~80	**0.34** **1.37**(patterned substrate)	This work
~50	~0.15	21
~50	~0.25	33
~100	~0.56	7
~100	~0.4	34
~100	~0.2	21
~100	~0.6	35
~200	~0.28	23
~200	~0.1	36
~200	~0.05	2
~200	~0.7	34
~200	~1.1	37
~200	~0.45	21
~270	~0.6	38
~270	~0.6	38
~300	~0.9	3
~370	~0.3	39
~600	~0.53	22
~700	~1.75	40

Figure 7. Comparison of the photocurrent density at 1.23 V_{RHE} of our ultrathin $BiVO_4$ photoanode with other pristine $BiVO_4$ photoanodes reported in the literature ordered by their film thickness. Solid fill bar: front illumination. Line fill bar: back illumination. Red dots: ultrathin $BiVO_4$ photoanodes (~80 nm) from this work with front illumination. The photocurrent density values and references are listed in the table next to the figure.

1.37 mA/cm^2 at 1.23 V_{RHE}, and it is further improved to 1.99 mA/cm^2 at 1.23 V_{RHE} by adding FeOOH OEC. The PEC performance of our ultrathin pristine $BiVO_4$ photoanode is comparable and better than most of the pristine $BiVO_4$ films in the literature. Our ultrathin $BiVO_4$ photoanode can be further enhanced by designing substrate patterns with more effective light-trapping schemes and introducing doping to improve charge transport efficiency. We believe that our transfer printing method will facilitate the integration of photoelectrodes and even other thin-film devices (e.g., solar cells, and electronics) with diverse textured rigid or flexible substrates for enhanced performance and broader applications.

■ ASSOCIATED CONTENT

Ⓢ Supporting Information

The Supporting Information is available free of charge on the ACS Publications website at DOI: 10.1021/acsenergylett.6b00032.

Experimental methods and additional information and figures (PDF)

■ AUTHOR INFORMATION

Corresponding Author

*E-mail: xlzheng@stanford.edu.

Author Contributions

J.Z. carried out the experiments for synthesis, transfer, and characterization of all photoanodes. J.Z. and X.Z. conceived the idea and wrote the manuscript. H.L. performed the AFM measurements. Y.G., K.W., and S.F. performed the numerical simulations for the optical part. L.C. and I.S.C. assisted in preparation of reagents for the synthesis and in the electrochemical characterization. C.H.L. assisted with the water-assisted transfer approach. All authors have commented on the manuscript.

Notes

The authors declare no competing financial interest.

■ ACKNOWLEDGMENTS

This work was funded by the Bay Area Photovoltaics Consortium (BAPVC). S.F. also acknowledges the support of the Department of Energy Grant DE-FG07ER46426.

■ REFERENCES

(1) Rao, P. M.; Cai, L. L.; Liu, C.; Cho, I. S.; Lee, C. H.; Weisse, J. M.; Yang, P. D.; Zheng, X. L. Simultaneously Efficient Light Absorption and Charge Separation in $WO_3/BiVO_4$ Core/Shell Nanowire Photoanode for Photoelectrochemical Water Oxidation. *Nano Lett.* **2014**, *14*, 1099−1105.

(2) Cho, S. K.; Park, H. S.; Lee, H. C.; Nam, K. M.; Bard, A. J. Metal Doping of $BiVO_4$ by Composite Electrodeposition with Improved Photoelectrochemical Water Oxidation. *J. Phys. Chem. C* **2013**, *117*, 23048−23056.

(3) Seabold, J. A.; Zhu, K.; Neale, N. R. Efficient Solar Photoelectrolysis by Nanoporous Mo: $BiVO_4$ through Controlled Electron Transport. *Phys. Chem. Chem. Phys.* **2014**, *16*, 1121−1131.

(4) Cai, L.; Cho, I. S.; Logar, M.; Mehta, A.; He, J.; Lee, C. H.; Rao, P. M.; Feng, Y.; Wilcox, J.; Prinz, F. B.; et al. Sol-Flame Synthesis of Cobalt-Doped TiO_2 Nanowires with Enhanced Electrocatalytic Activity for Oxygen Evolution Reaction. *Phys. Chem. Chem. Phys.* **2014**, *16*, 12299−12306.

(5) Cho, I. S.; Lee, C. H.; Feng, Y.; Logar, M.; Rao, P. M.; Cai, L.; Kim, D. R.; Sinclair, R.; Zheng, X. Codoping Titanium Dioxide Nanowires with Tungsten and Carbon for Enhanced Photoelectrochemical Performance. *Nat. Commun.* **2013**, *4*, 1723.

(6) Cho, I. S.; Logar, M.; Lee, C. H.; Cai, L.; Prinz, F. B.; Zheng, X. Rapid and Controllable Flame Reduction of TiO_2 Nanowires for Enhanced Solar Water-Splitting. *Nano Lett.* **2014**, *14*, 24−31.

(7) Abdi, F. F.; Dabirian, A.; Dam, B.; van de Krol, R. Plasmonic Enhancement of the Optical Absorption and Catalytic Efficiency of $BiVO_4$ Photoanodes Decorated with $Ag@SiO_2$ Core-Shell Nanoparticles. *Phys. Chem. Chem. Phys.* **2014**, *16*, 15272−15277.

(8) Zhang, L.; Lin, C. Y.; Valev, V. K.; Reisner, E.; Steiner, U.; Baumberg, J. J. Plasmonic Enhancement in $BiVO_4$ Photonic Crystals for Efficient Water Splitting. *Small* **2014**, *10*, 3970−3978.

(9) Sun, K.; Shen, S.; Liang, Y.; Burrows, P. E.; Mao, S. S.; Wang, D. Enabling Silicon for Solar-Fuel Production. *Chem. Rev.* **2014**, *114*, 8662−8719.

(10) Noh, J. H.; Ding, B.; Han, H. S.; Kim, J. S.; Park, J. H.; Park, S. B.; Jung, H. S.; Lee, J. K.; Hong, K. S. Tin Doped Indium Oxide Core-TiO_2 Shell Nanowires on Stainless Steel Mesh for Flexible Photoelectrochemical Cells. *Appl. Phys. Lett.* **2012**, *100*, 084104.

(11) Lee, S.; Park, S.; Han, G. S.; Kim, D. H.; Noh, J. H.; Cho, I. S.; Jung, H. S.; Hong, K. S. Transparent-Conducting-Oxide Nanowire Arrays for Efficient Photoelectrochemical Energy Conversion. *Nanoscale* **2014**, *6*, 8649−8655.

(12) Dotan, H.; Kfir, O.; Sharlin, E.; Blank, O.; Gross, M.; Dumchin, I.; Ankonina, G.; Rothschild, A. Resonant Light Trapping in Ultrathin Films for Water Splitting. *Nat. Mater.* **2013**, *12*, 158−164.

DOI: 10.1021/acsenergylett.6b00032
ACS Energy Lett. 2016, 1, 68−75

(13) Kim, S. J.; Thomann, I.; Park, J.; Kang, J.-H.; Vasudev, A. P.; Brongersma, M. L. Light Trapping for Solar Fuel Generation with Mie Resonances. *Nano Lett.* **2014**, *14*, 1446−1452.
(14) Li, J.; Qiu, Y.; Wei, Z.; Lin, Q.; Zhang, Q.; Yan, K.; Chen, H.; Xiao, S.; Fan, Z.; Yang, S. A Three-Dimensional Hexagonal Fluorine-Doped Tin Oxide Nanocone Array: A Superior Light Harvesting Electrode for High Performance Photoelectrochemical Water Splitting. *Energy Environ. Sci.* **2014**, *7*, 3651−3658.
(15) Qiu, Y.; Leung, S.-F.; Zhang, Q.; Hua, B.; Lin, Q.; Wei, Z.; Tsui, K.-H.; Zhang, Y.; Yang, S.; Fan, Z. Efficient Photoelectrochemical Water Splitting with Ultrathin Films of Hematite on Three-Dimensional Nanophotonic Structures. *Nano Lett.* **2014**, *14*, 2123−2129.
(16) Lee, C. H.; Kim, D. R.; Cho, I. S.; William, N.; Wang, Q.; Zheng, X. L. Peel-and-Stick: Fabricating Thin Film Solar Cell on Universal Substrates. *Sci. Rep.* **2012**, *2*, 1000.
(17) Lee, C. H.; Kim, D. R.; Zheng, X. L. Fabrication of Nanowire Electronics on Nonconventional Substrates by Water-Assisted Transfer Printing Method. *Nano Lett.* **2011**, *11*, 3435−3439.
(18) Wang, L.; Lee, C. Y.; Schmuki, P. Solar Water Splitting: Preserving the Beneficial Small Feature Size in Porous Alpha-Fe_2O_3 Photoelectrodes During Annealing. *J. Mater. Chem. A* **2013**, *1*, 212−215.
(19) Abdi, F. F.; Savenije, T. J.; May, M. M.; Dam, B.; van de Krol, R. The Origin of Slow Carrier Transport in $BiVO_4$ Thin Film Photoanodes: A Time-Resolved Microwave Conductivity Study. *J. Phys. Chem. Lett.* **2013**, *4*, 2752−2757.
(20) Liang, Y.; Tsubota, T.; Mooij, L. P. a.; Van De Krol, R. Highly Improved Quantum Efficiencies for Thin Film $BiVO_4$ Photoanodes. *J. Phys. Chem. C* **2011**, *115*, 17594−17598.
(21) Bornoz, P.; Abdi, F. F.; Tilley, S. D.; Dam, B.; van de Krol, R.; Graetzel, M.; Sivula, K. A Bismuth Vanadate−Cuprous Oxide Tandem Cell for Overall Solar Water Splitting. *J. Phys. Chem. C* **2014**, *118*, 16959−16966.
(22) Zhang, L. W.; Reisner, E.; Baumberg, J. J. Al-Doped ZnO Inverse Opal Networks as Efficient Electron Collectors in $BiVO_4$ Photoanodes for Solar Water Oxidation. *Energy Environ. Sci.* **2014**, *7*, 1402−1408.
(23) Alarcon-Llado, E.; Chen, L.; Hettick, M.; Mashouf, N.; Lin, Y.; Javey, A.; Ager, J. W. $BiVO_4$ Thin Film Photoanodes Grown by Chemical Vapor Deposition. *Phys. Chem. Chem. Phys.* **2014**, *16*, 1651−1657.
(24) Cho, I. S.; Han, H. S.; Logar, M.; Park, J.; Zheng, X. Enhancing Low-Bias Performance of Hematite Photoanodes for Solar Water Splitting by Simultaneous Reduction of Bulk, Interface, and Surface Recombination Pathways. *Adv. Energy Mater.* **2016**, *6*, 1501840.
(25) Li, H.; Contryman, A. W.; Qian, X.; Ardakani, S. M.; Gong, Y.; Wang, X.; Weisse, J. M.; Lee, C. H.; Zhao, J.; Ajayan, P. M.; et al. Optoelectronic Crystal of Artificial Atoms in Strain-Textured Molybdenum Disulphide. *Nat. Commun.* **2015**, *6*, 7381.
(26) Ma, Y.; Pendlebury, S. R.; Reynal, A.; Le Formal, F.; Durrant, J. R. Dynamics of Photogenerated Holes in Undoped $BiVO_4$ Photoanodes for Solar Water Oxidation. *Chem. Sci.* **2014**, *5*, 2964−2973.
(27) Liu, V.; Fan, S. S4: A Free Electromagnetic Solver for Layered Periodic Structures. *Comput. Phys. Commun.* **2012**, *183*, 2233−2244.
(28) Kibsgaard, J.; Jaramillo, T. F. Molybdenum Phosphosulfide: An Active, Acid-Stable, Earth-Abundant Catalyst for the Hydrogen Evolution Reaction. *Angew. Chem., Int. Ed.* **2014**, *53*, 14433−14437.
(29) He, W.; Wang, R.; Zhou, C.; Yang, J.; Li, F.; Xiang, X. Controlling the Structure and Photoelectrochemical Performance of $BiVO_4$ Photoanodes Prepared from Electrodeposited Bismuth Precursors: Effect of Zinc Ions as Directing Agent. *Ind. Eng. Chem. Res.* **2015**, *54*, 10723−10730.
(30) Pyper, K. J.; Yourey, J. E.; Bartlett, B. M. Reactivity of $CuWO_4$ in Photoelectrochemical Water Oxidation Is Dictated by a Midgap Electronic State. *J. Phys. Chem. C* **2013**, *117*, 24726−24732.
(31) Reddy, A. S.; Figueiredo, N. M.; Cavaleiro, A. Nanocrystalline SnO_2 and Au:SnO_2 Thin Films Prepared by Direct Current Magnetron Reactive Sputtering. *Vacuum* **2012**, *86*, 1323−1327.
(32) Li, R.; Zhang, F.; Wang, D.; Yang, J.; Li, M.; Zhu, J.; Zhou, X.; Han, H.; Li, C. Spatial Separation of Photogenerated Electrons and Holes among {010} and {110} Crystal Facets of $BiVO_4$. *Nat. Commun.* **2013**, *4*, 1432.
(33) McDowell, M. T.; Lichterman, M. F.; Spurgeon, J. M.; Hu, S.; Sharp, I. D.; Brunschwig, B. S.; Lewis, N. S. Improved Stability of Polycrystalline Bismuth Vanadate Photoanodes by Use of Dual-Layer Thin TiO_2/Ni Coatings. *J. Phys. Chem. C* **2014**, *118*, 19618−19624.
(34) Abdi, F. F.; Firet, N.; vandeKrol, R. Efficient $BiVO_4$ Thin Film Photoanodes Modified with Cobalt Phosphate Catalyst and W-Doping. *ChemCatChem* **2013**, *5*, 490−496.
(35) Abdi, F. F.; van de Krol, R. Nature and Light Dependence of Bulk Recombination in Co-Pi-Catalyzed $BiVO_4$ Photoanodes. *J. Phys. Chem. C* **2012**, *116*, 9398−9404.
(36) Ho-Kimura, S.; Moniz, S. J. a.; Handoko, A. D.; Tang, J. Enhanced Photoelectrochemical Water Splitting by Nanostructured $BiVO_4$−TiO_2 Composite Electrodes. *J. Mater. Chem. A* **2014**, *2*, 3948−3953.
(37) Abdi, F. F.; Han, L. H.; Smets, A. H. M.; Zeman, M.; Dam, B.; van de Krol, R. Efficient Solar Water Splitting by Enhanced Charge Separation in a Bismuth Vanadate-Silicon Tandem Photoelectrode. *Nat. Commun.* **2013**, *4*, 2195.
(38) Saito, R.; Miseki, Y.; Sayama, K. Highly Efficient Photoelectrochemical Water Splitting Using a Thin Film Photoanode of $BiVO_4$/SnO_2/WO_3 Multi-Composite in a Carbonate Electrolyte. *Chem. Commun.* **2012**, *48*, 3833−3835.
(39) Luo, W.; Wang, J.; Zhao, X.; Zhao, Z.; Li, Z.; Zou, Z. Formation Energy and Photoelectrochemical Properties of $BiVO_4$ after Doping at Bi^{3+} or V^{5+} Sites with Higher Valence Metal Ions. *Phys. Chem. Chem. Phys.* **2013**, *15*, 1006−1013.
(40) Kim, T. W.; Choi, K. S. Nanoporous $BiVO_4$ Photoanodes with Dual-Layer Oxygen Evolution Catalysts for Solar Water Splitting. *Science* **2014**, *343*, 990−994.

DOI: 10.1021/acsenergylett.6b00032
ACS Energy Lett. 2016, 1, 68−75